A major purpose of the Technical Information Center is to provide the broadest dissemination possible of information contained in DOE's Research and Development Reports to business, industry, the academic community, and federal, state and local governments.

Although a small portion of this report is not reproducible, it is being made available to expedite the availability of information on the research discussed herein.

1

LA-UR -84-2479

CONF-840806--8

LA-UR--84-2479

DE84 016485

TITLE: FIRE SIMULATION IN NUCLEAR FACILITIES--
THE FIRAC CODE AND SUPPORTING EXPERIMENTS

AUTHOR(S): M. W. Burkett
R. A. Martin
D. L. Fenton
M. V. Gunaji

SUBMITTED TO: 18th DOE Nuclear Airborne Waste Management and Air Cleaning Conference, Baltimore, MD, August 14-16, 1984.

DISCLAIMER

Los Alamos National Laboratory
Los Alamos, New Mexico 87545

FIRE SIMULATION IN NUCLEAR FACILITIES-- THE FIRAC CODE AND SUPPORTING EXPERIMENTS

M. W. Burkett and R. A. Martin
Los Alamos National Laboratory
Los Alamos, New Mexico

D. L. Fenton and M. V. Gunaji
New Mexico State University
Las Cruces, New Mexico

Abstract

The fire accident analysis computer code FIRAC was designed to estimate radioactive and nonradioactive source terms and predict fire-induced flows and thermal and material transport within the ventilation systems of nuclear fuel cycle facilities. FIRAC maintains its basic structure and features and has been expanded and modified to include the capabilities of the zone-type compartment fire model computer code FIRIN developed by Battelle Pacific Northwest Laboratory. The two codes have been coupled to provide an improved simulation of a fire-induced transient within a facility. The basic material transport capability of FIRAC has been retained and includes estimates of entrainment, convection, deposition, and filtration of material. The interrelated effects of filter plugging, heat transfer, gas dynamics, material transport, and fire and radioactive source terms also can be simulated. Also, a sample calculation has been performed to illustrate some of the capabilities of the code and how a typical facility is modeled with FIRAC.

In addition to the analytical work being performed at Los Alamos, experiments are being conducted at the New Mexico State University to support the FIRAC computer code development and verification. This paper summarizes two areas of the experimental work that support the material transport capabilities of the code: the plugging of high-efficiency particulate air (HEPA) filters by combustion aerosols and the transport and deposition of smoke in ventilation system ductwork.

I. Introduction

The development of the FIRAC computer code and the supporting experimental work are being sponsored by the Nuclear Regulatory Commission (NRC). The NRC is responsible for ensuring that nuclear fuel cycle facilities are designed and operated in a safe manner so that the release of radioactive material under both normal and accident conditions will not result in unacceptable radiological effects on the surrounding population and the environment.[1]

The NRC requested the original FIRAC computer code be modified and expanded to include the capabilities of the zone-type compartment fire model FIRIN, which was developed by Battelle Pacific Northwest Laboratories (PNL). The two codes have been coupled to allow an improved simulation of a fire-induced transient within a facility.

The expanded version of FIRAC is designed to predict the radioactive and nonradioactive source terms that lead to gas dynamics, material transport, and heat transfer transients in a nuclear facility when it is subjected to a fire. The code is directed toward nuclear fuel cycle facilities and the primary release pathway--the ventilation system. However, the code is applicable to other facilities and can be used to model other airflow pathways within a structure.

The physical models used in the code may be divided into four principal categories.

- Gas dynamics model
- Material transport models
- Heat transfer models
- FIRIN fire and radioactive source term models

A brief summary of the gas dynamics, convective material transport capabilities, heat transfer capabilities, and FIRIN source term models is presented. Details of the gas dynamics, material transport, and heat transfer capabilities can be found in Reference 2. More information on the FIRIN source terms is provided in Reference 3.

In addition to the FIRIN fire compartment option, the code allows the user to employ any fire compartment model provided that the output of the compartment model is in one of two forms:

- pressure and temperature time histories or
- energy and mass time histories.

An application of the code using the FIRIN source term models to a typical nuclear facility is presented, as is a summary of experiments in two areas that support the development and verification of FIRAC. The two areas of experimental support are: high-efficiency particulate air (HEPA) filter plugging by combustion aerosols and smoke transport and deposition in ventilation system ductwork.

Physical Models

The lumped-parameter method is the basic formulation that describes the airflow system. No spatial distribution of parameters is considered in this approach, but an effect of spatial distribution can be approximated by noding. Network theory, using the lumped-parameter method, includes a number of system elements called branches joined at certain points called nodes. Ventilation system components that exhibit flow resistance and inertia (such as dampers, ducts, valves, and filters) and that exhibit flow potential (such as blowers) are located within the branches of the system.

Nodes are the connection points of branches for components that have finite volumes, such as rooms, gloveboxes, and plenums, and for boundaries where the volume is practically infinite. When the FIRIN source-term models are selected to simulate a fire accident, internal boundary nodes are used to represent the fire compartment within the ventilation network. Even though they are zero-volume nodes within the numerical scheme, the fact that they are coupled to a fire compartment model that accounts for mass and energy balances keeps the computational formulation consistent.

Material Transport Models

The object of the material transport portion of the code is to estimate the movement of material (aerosol or gas) in an interconnected network of ventilation system components representing a given fuel cycle facility. Using this capability, the code can calculate material concentrations and material mass flow rates at any location in the network. Furthermore, the code will perform these transport calculations for various gas-dynamic transients. The code solves the entire network for transient flow and in so doing takes into account system interactions.

A generalized treatment of material transport under fire-induced accident conditions could become very complex. Several different types of materials could be transported. Also, more than one phase could be involved, including solids, liquids, and gases with phase transitions. Chemical reactions could occur during transport, leading to the formation of new species. Further, for each type of material there will be a size distribution that varies with time and position depending on the relative importance of effects such as homogeneous nucleation, coagulation (material interaction), diffusion (both by Brownian motion and by turbulence), and gravitational sedimentation. We know of no codes that can handle transient flow induced material transport in a network system subject to the possibility of all of these complications. The transport portion of the code also does not include this level of generality. However, this version of the code does provide a simple material transport capability.

The material transport components of this code consist of the following.

1. Material characteristics
2. Transport initiation
3. Convective transport
4. Aerosol depletion
5. Filtration

Material characteristics and transport initiation are areas that must be considered by the user as he begins to set up the code to solve a given problem. Calculations of convective transport, aerosol depletion, and filtration are performed automatically by the code. Items 2--5 are actually separate subroutines or modules within the code. Item 3, convective transport, is a key subroutine that calls on items 2, 4, and 5 as needed during the course of the calculation. We also will specify the required user specifications and provide appropriate references for the theory in each case.

Duct Heat Transfer

The purpose of the duct heat transfer model is to predict how the combustion gas in the system heats up or cools down as it flows throughout the ducts in the ventilating system. The model predicts the temperature of the gas leaving any section of the duct if the inlet temperature and gas properties are known. An ancillary result

of the calculations yields the duct wall temperature. A duct component is the only one for which a heat transfer calculation is performed. Furthermore, the calculation is performed in a given duct only if that branch has been flagged in the user specifications. Experience in using the code has shown that duct heat transfer calculations can increase the computer running time by a factor of 2. Therefore, we advise that duct heat transfer calculations be performed only where needed. The main region of interest and concern is generally those ducts downstream from the fire compartment and especially between the fire compartment and any filters downstream from the fire compartment.

The overall model is composed of five distinct sub-models of heat transfer processes along with a numerical solution procedure to evaluate them. The heat transfer processes modeled are the following.

- Forced convection heat transfer between the combustion gas and the inside duct walls.
- Radiation heat transfer between the combustion gas and inside duct walls
- Heat conduction through the duct wall
- Natural convection heat transfer from the outside duct walls to the surroundings
- Radiation heat transfer from the outside duct walls to the atmosphere

FIRIN Fire and Radioactive Source Term Simulation

Accidental fire-generated radioactive and nonradioactive source terms for nuclear facilities are estimated in the FIRIN module of the FIRAC code. FIRIN uses a zone-type compartment fire model. A zone-type fire compartment assumes that the gas in the room is divided into two homogeneous regions, or layers, during a fire. One layer (the hot layer) develops near the ceiling and contains the hot combustion products released from the burning material. The cold layer, which is located between the hot layer and the floor, contains fresh air. FIRIN predicts the fire source mass loss rate, energy generation rate, and fire room conditions (temperatures of the two layers and room pressure) as a function of time. It also calculates the mass generation rate and particle size distributions for radioactive and nonradioactive particles that can become airborne for a given fire accident scenario. The radioactive release factors incorporated within the FIRIN module are primarily those developed in experimental work at PNL, and the combustion product data were developed from a literature search of combustibles that commonly are found in nuclear facilities. More information on the fire and radioactive source term models and FIRIN code assumptions is available in Reference 3.

Fire Accident Analysis Example

Description and Computer Model of the Facility. This example calculation will illustrate how the improved fire code can be applied to a complex facility as shown in Figure 1. This facility is representative of most nuclear fuel cycle ventilation systems in that it contains multiple fans, compartments, dampers, filter systems, and parallel/series flow configurations. The facility model features 39 branches, 24 nodes [19 capacitance (room) nodes, 2 standard boundary nodes, and 3 internal boundary nodes], 2 blowers, and 9 filters. For this calculation, the FIRIN fire compartment model is used to characterize the nonradioactive and radioactive source terms resulting from the fire. Within the facility ventilation network, internal boundary nodes 9, 21, and 22 represent the fire compartment. (A closeup of the fire compartment noding is shown in Figure 2.) The inlet and outlet branches (connections) to the fire compartment have been positioned so that the ventilation flow direction is downward in the room. That is, the inlet is located near the ceiling, and the outlet is near the floor.

The fire compartment is assumed to be 39 ft (12 m) long, 39 ft (12 m) wide, and 20 ft (6 m) high. The centerline elevation (measured from the floor) of the two inlet vents is 18.74 ft (5.71 m), and the elevation of the outlet vent is 3.0 ft (0.9 m). Also, the fire compartment is assumed to have a concrete floor, ceiling, and walls. The ceiling and floor are assumed to be 1.0 ft (0.3 m) thick; the walls are assumed to be 0.5 ft (0.2 m) thick.

When the system is operating under steady-state conditions, the fire compartment has a pressure of -0.30 in. w.g. (-0.76 cm w.g.) at a temperature of 70°F (21°C). The two inlet vents (branches 16 and 17) supply 3250 ft^3/min (1.534 m^3/s) and 300 ft^3/min (0.141 m^3/s) of air to the compartment. The outlet ventilator exhausts 3550 ft^3/min (1.675 m^3/s) under steady-state conditions. The fire compartment exhaust filter (branch 14) is assumed to be 50% efficient and have a plugging factor of 10.0 1/kg. A low fire compartment exhaust filter efficiency was selected to illustrate the transport of particulate material to the facility exhaust filter and the potential for deposition of material in the two ducts (branches 38 and 39) located downstream of the fire compartment (Figure 2).

Fire Accident Scenario

In defining an accident scenario, the combustible materials susceptible to ignition and the radioactive materials at risk must be identified. For a compartment fire, typical combustible materials are elastomers (neoprene gloves), cellulosic materials (rags, paper, wood), flammable and combustible liquids (solvents and hydraulic oil), and plastic (polymethylmethacrylate and polyvinyl chloride). The materials at risk could include contaminated noncombustible surfaces, contaminated combustible liquids and solids, and open containers of divided powders or liquids. After the amount and type of

REPRESENTATIVE FACILITY

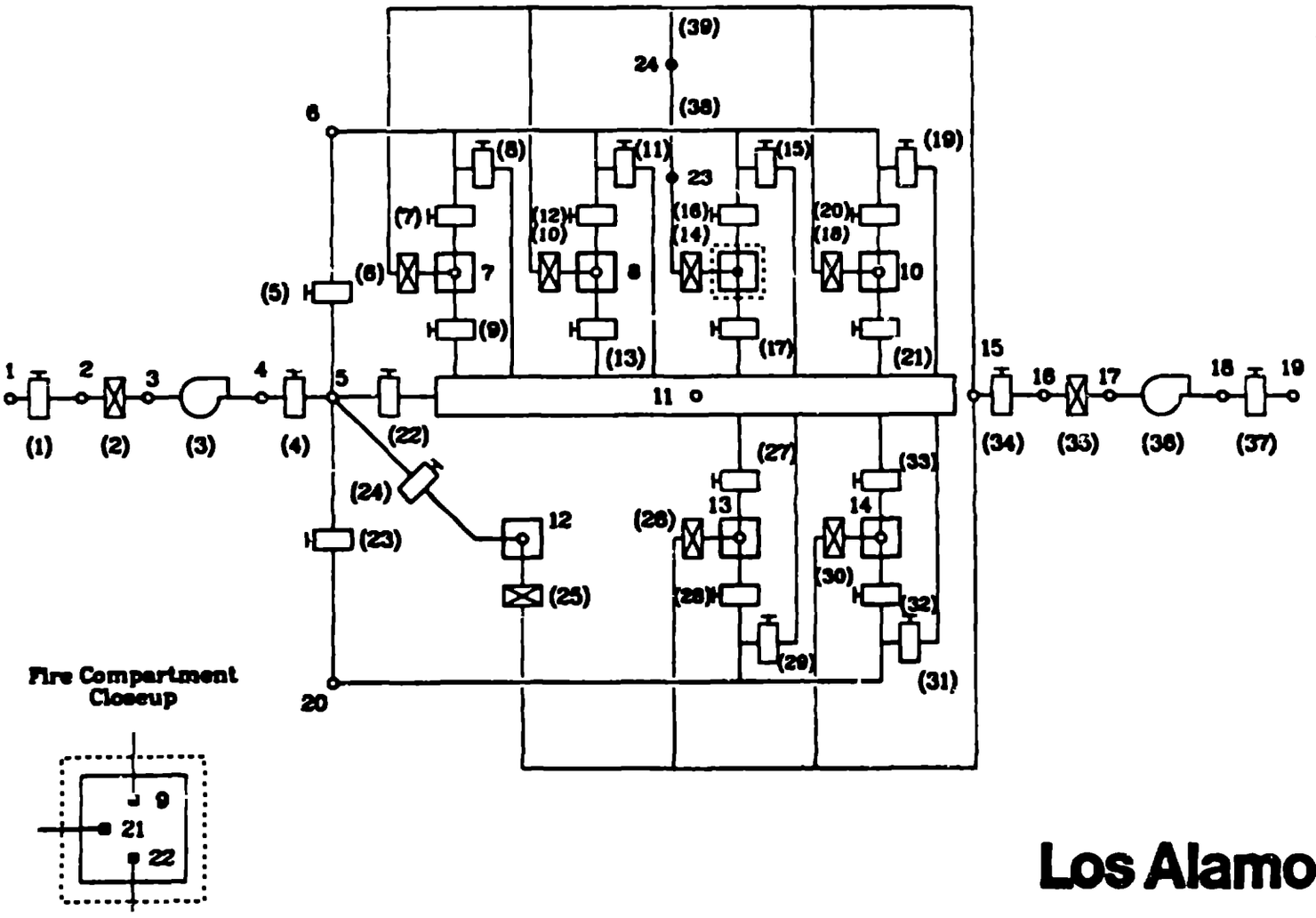

Figure 1. Representative facility ventilation system schematic.

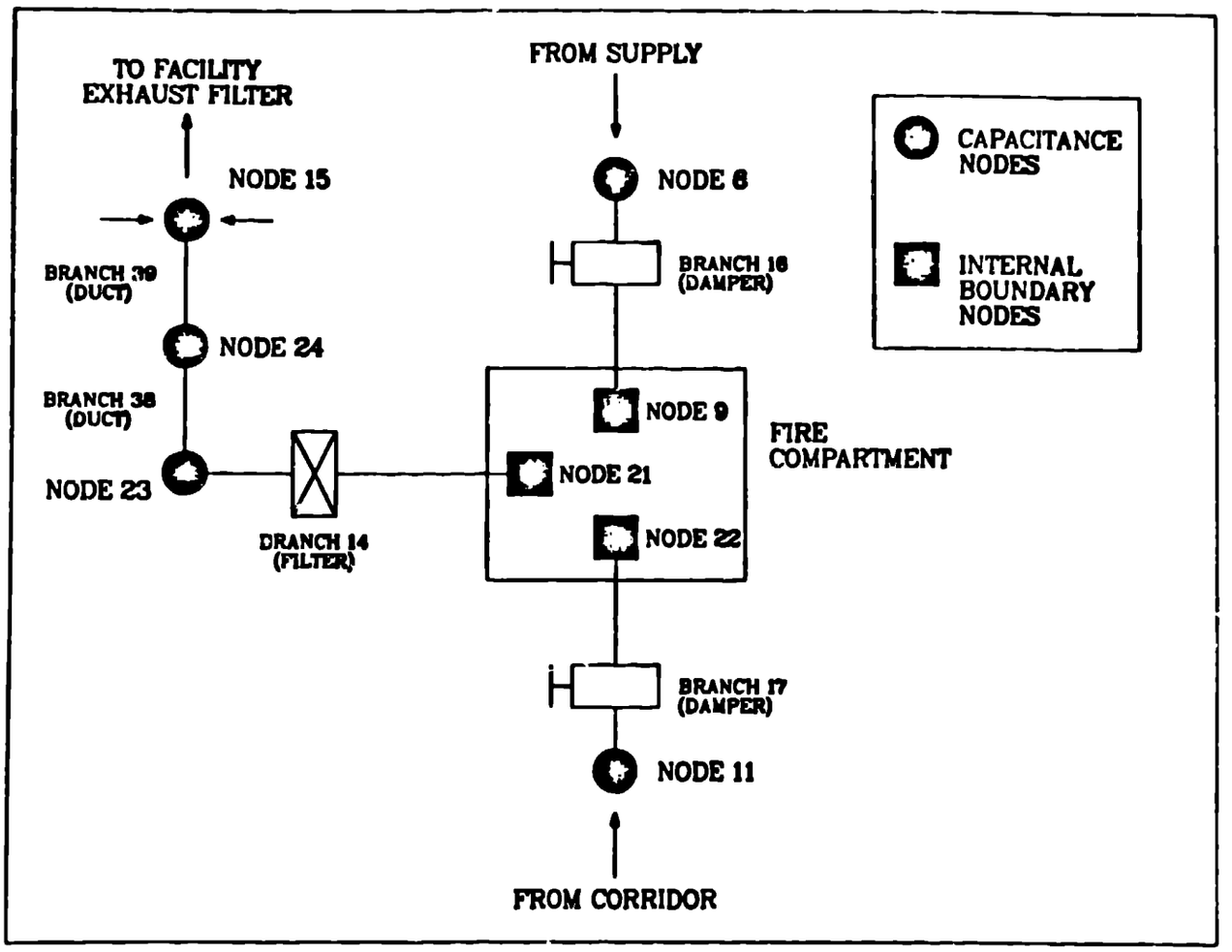

Figure 2. Closeup system schematic near the fire compartment.

combustibles and at-risk radioactive materials have been identified, the fire growth sequence (the order in which the combustible materials are assumed to burn) can be formulated. It is recognized that fire accidents most probably occur under abnormal operating conditions (spilled combustibles or improper use of solvents) or from unanticipated events (failed electrical equipment or faulty processing equipment).

For the sample calculation two combustibles are assumed to be at risk within the fire compartment: a container of flammable solvent (kerosene) and several pairs of rubber (polychloroprene) gloves. The fire begins after the solvent container overturns and is accidentally ignited. The rubber gloves are assumed to be located near the overturned solvent. As the solvent burns, the gloves are gradually heated and ignite as the solvent stops burning. The spilled solvent is assumed to have an exposed surface (burn) area of 5.0 ft^2 (0.5 m^2) and an initial mass of 3.0 lbm (1.4 kg). The rubber gloves are assumed to have an exposed surface area of 4.0 ft^2 (1.8 m^2) and an initial mass of 8.1 lbm (3.6 kg). The FIRIN sequential burning option was used to achieve the fire growth sequence described above.

Two mechanisms for the release of radioactive material located within the fire compartment are used in the example calculation: the release of material associated with the heating of contaminated surfaces and of material associated with the burning of a contaminated combustible solid. The fire compartment floor and walls are assumed to be contaminated with 0.165 lbm (0.075 kg) of mixed oxide powder. In addition to the fixed surface contamination, the combustible polychloroprene gloves are contaminated with 0.033 lbm (0.015 kg) of mixed oxide powder. The radioactive particulate release rates for the single nonradioactive (smoke generation rate) and the two radioactive release mechanisms are calculated within the FIRIN module.

Calculative Results

The sequence of events for the example calculation is presented in Table 1. The kerosene ignition initiates the accident sequence 2 s into the simulation. The fire compartment (represented by nodes 9, 21, and 22 in the system model) rapidly pressurizes from its steady-state operating value of -0.30 in. w.g. (-0.76 cm w.g.) to approximately 0.55 in. w.g. (1.40 cm w.g.) because of the rapid volumetric expansion of the compartment gases caused by the fire. Figure 3 shows the fire compartment pressure response for the entire transient. As a result of the pressure increase in the compartment, a reduction in flow at the intakes (branches 16 and 17) and an increase in flow at the compartment exhaust (branch 14) is calculated by FIRAC. Volumetric flow rate results for the fire compartment are presented in Figure 4.

Between 2 s and 175 s, the hot layer gradually expands and descends toward the outflow ventilator (Figure 5). As the outflow ventilator begins to exhaust the hot combustion products/gases composing the hot layer, the fire compartment begins to depressurize

Table 1. Transient event sequence for example calculation.

Event	Time (s)
Kerosene ignites	2
Maximum system temperature (150°F) attained	5
Hot layer descends to centerline elevation of inflow boundaries	15
Hot layer descends to centerline elevation of outflow boundary	205
Contaminated polychloroprene ignites	275
Radioactive material appears in system	275
Polychloroprene stops burning	350
End of calculation	500

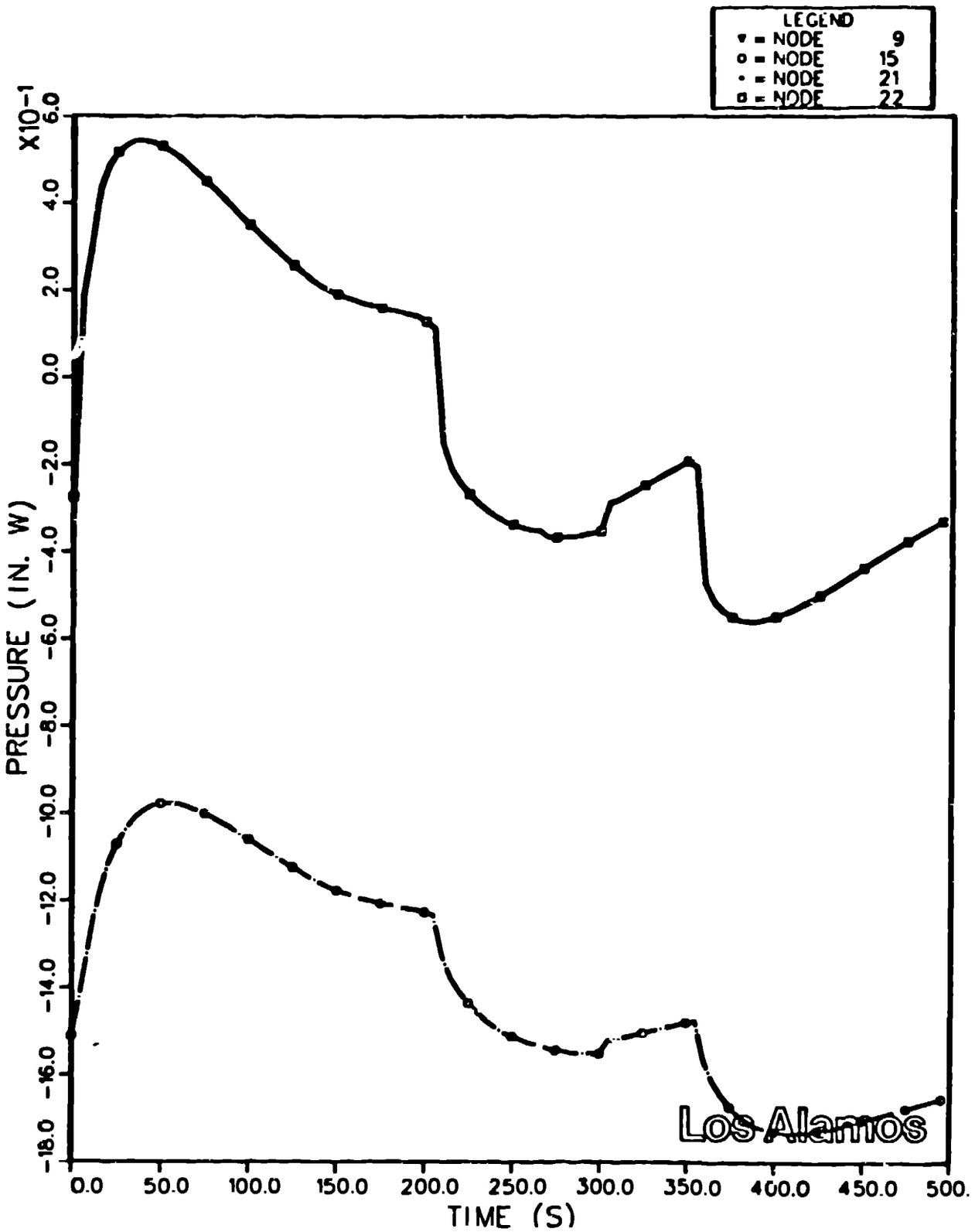

Figure 5. Calculated pressure response for nodes 9, 15, 21, and 22.

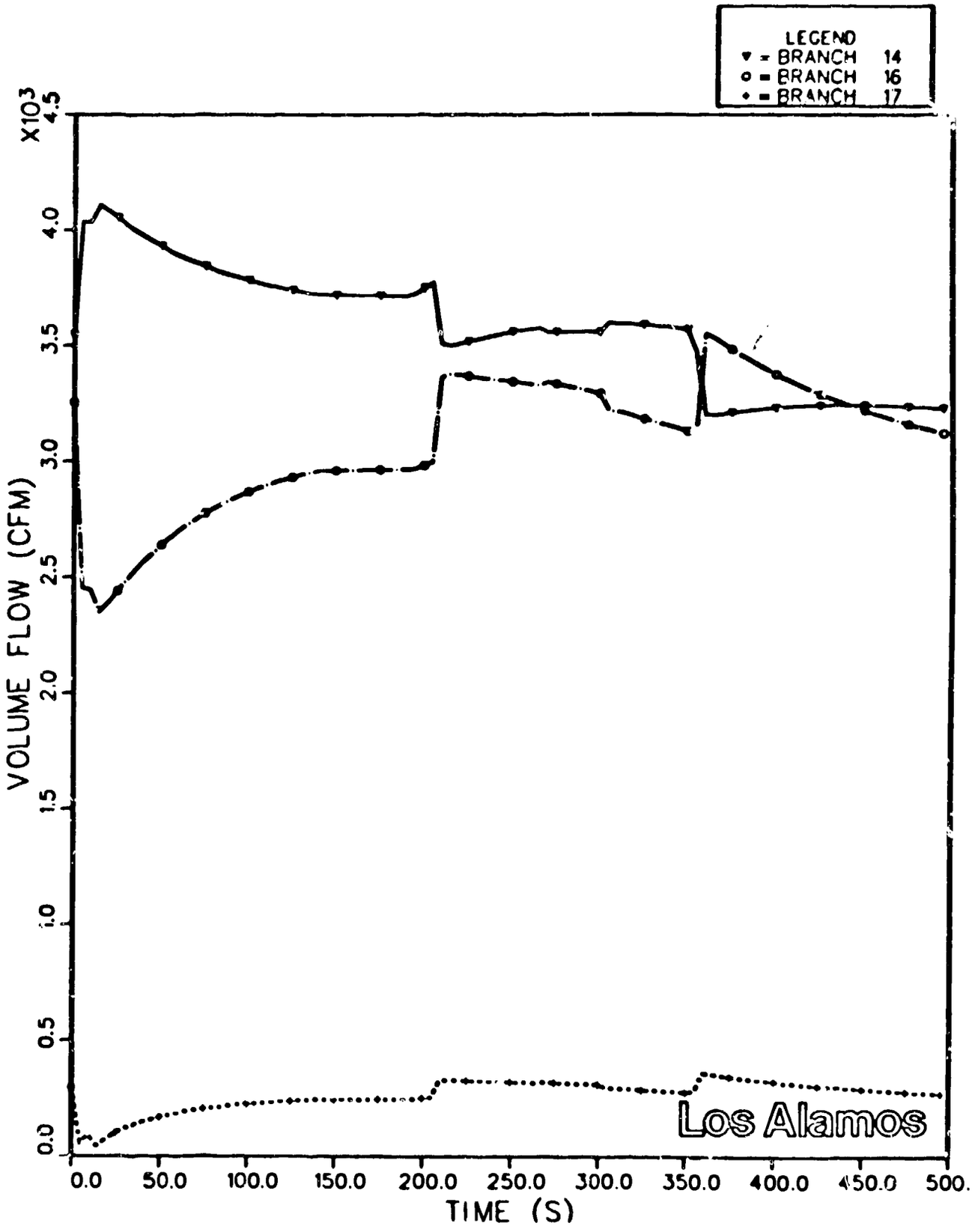

Figure 4. Calculated for compartment volumetric flow rates (branches 14, 16, and 17).

slightly. The volumetric and mass flows at the intakes to the compartment are enhanced by the depressurization. The compartment exhaust flow rate decreased because of the depressurization and the presence of the hot (less dense) combustion gases at the outflow ventilator. The temperature history for the fire compartment is shown in Figure 6.

The system is perturbed again as the kerosene fire terminates and the contaminated polychloroprene ignites via the sequential burning option. The ignition of the polychloroprene repressurizes the fire compartment to -0.2 in. w.g. (-0.5 cm w.g.) by 350 s. The flow rates to the compartment are affected by the repressurization: the exhaust flow (branch 14) is enhanced and flow at the intakes (branches 16 and 17) is reduced. As the polychloroprene burns, the compartment becomes more filled with smoke particulates because burning polystyrene releases a larger amount of smoke particulate than does burning kerosene.

The production of smoke at a faster rate within the compartment begins to deplete the amount of oxygen available to the fire. The fire compartment oxygen concentration never dropped below 20% because the polychloroprene burned for only a short time (90 s). By 355 s, all the combustible materials within the compartment have been consumed and the system begins to recover from the fire-induced transient.

Even though the filter plugging option was used in the calculation, the fire compartment exhaust filter does not plug and therefore does not influence the system response to the fire. The low fire compartment filter efficiency (50%) prevents the filter from collecting enough mass to plug. However, the low efficiency value does allow smoke and radioactive material to be transported to the facility exhaust filter (branch 35). Figures 7 and 8 show the mass accumulations for the smoke and total radioactive particulates on the fire compartment exhaust filter (branch 14), the two ducts located between the compartment exhaust filter, the facility exhaust filter (branches 38 and 39), and the facility exhaust filter (branch 35).

The primary release mechanism for radioactive material is the burning of a contaminated combustible solid (polychloroprene). The releases associated with the heating of a contaminated surface are simulated in this calculation but are not evident in the mass accumulation results (Figure 8). Once the hot layer has descended to the outflow elevation, material released as a result of the contaminated surface being heated is convected through the system. The release rates for the contaminated surface mechanism are several orders of magnitude less than the release rates for the burning contaminated combustible. Significant quantities of radioactive material are not transported until the polychloroprene ignites at 275 s. The polychloroprene is assumed to ignite after the kerosene pool fire has ended.

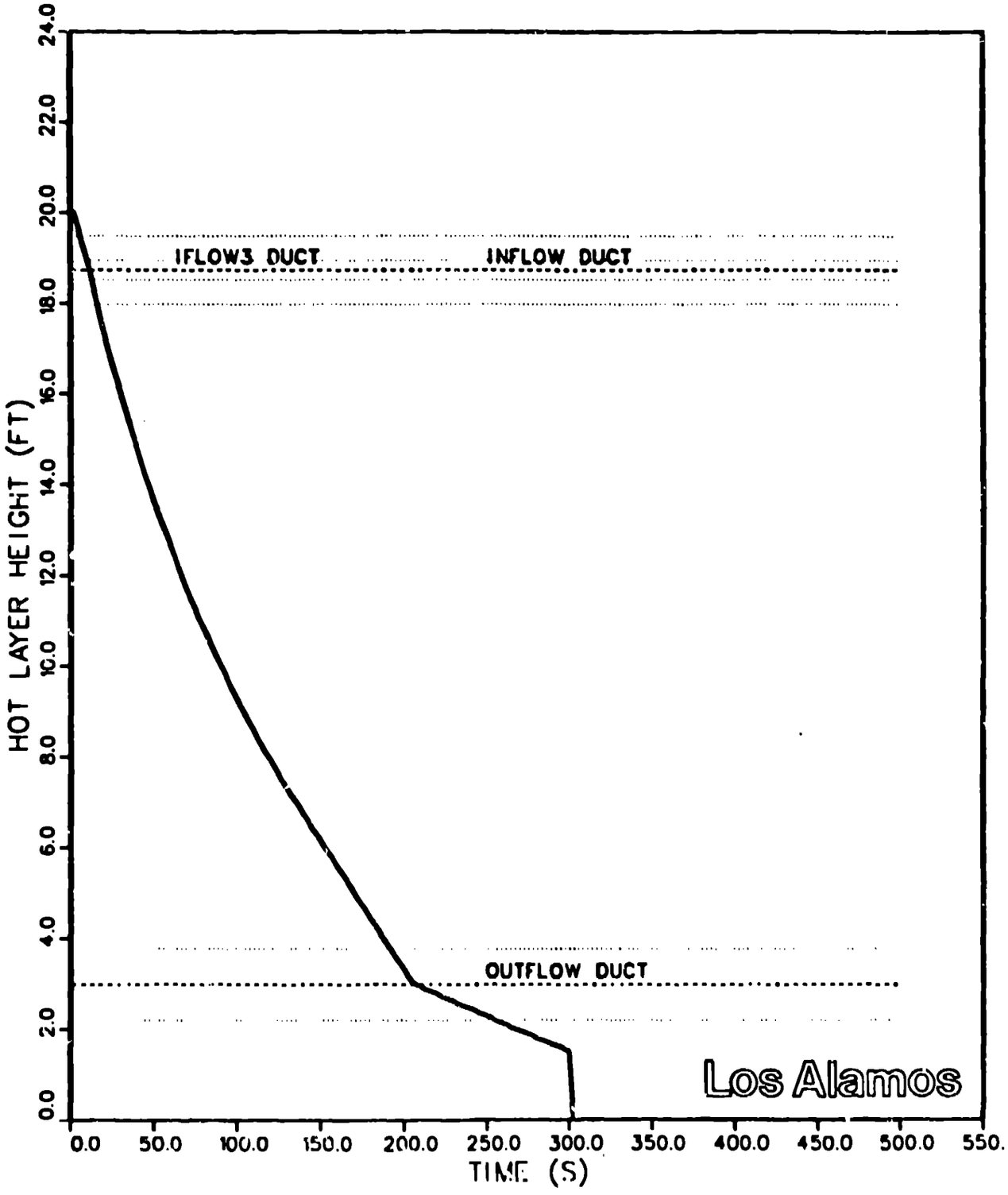

Figure 5. Calculated hot layer height versus time.

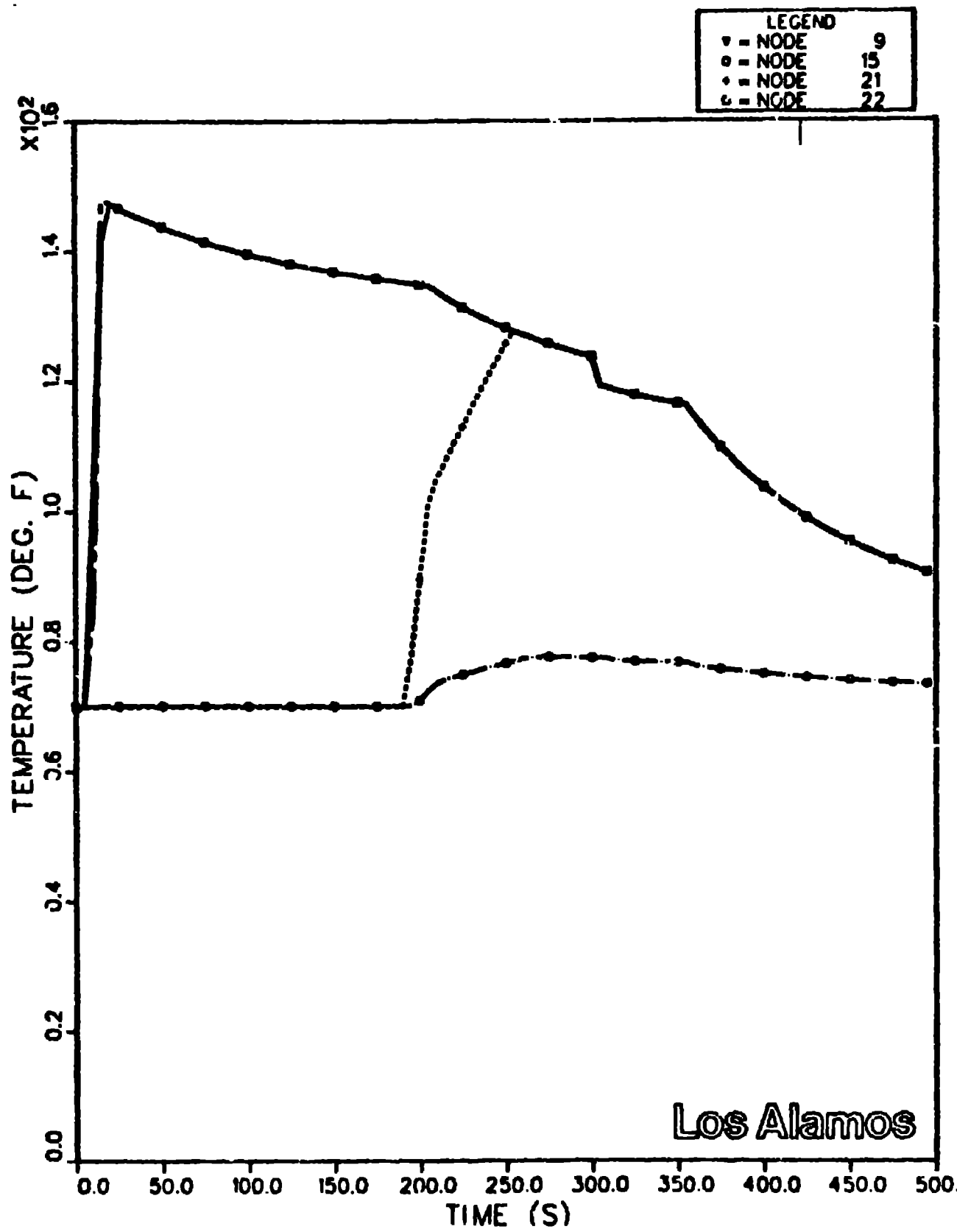

Figure 6. Calculated temperature history for nodes 9, 15, 21, and 22.

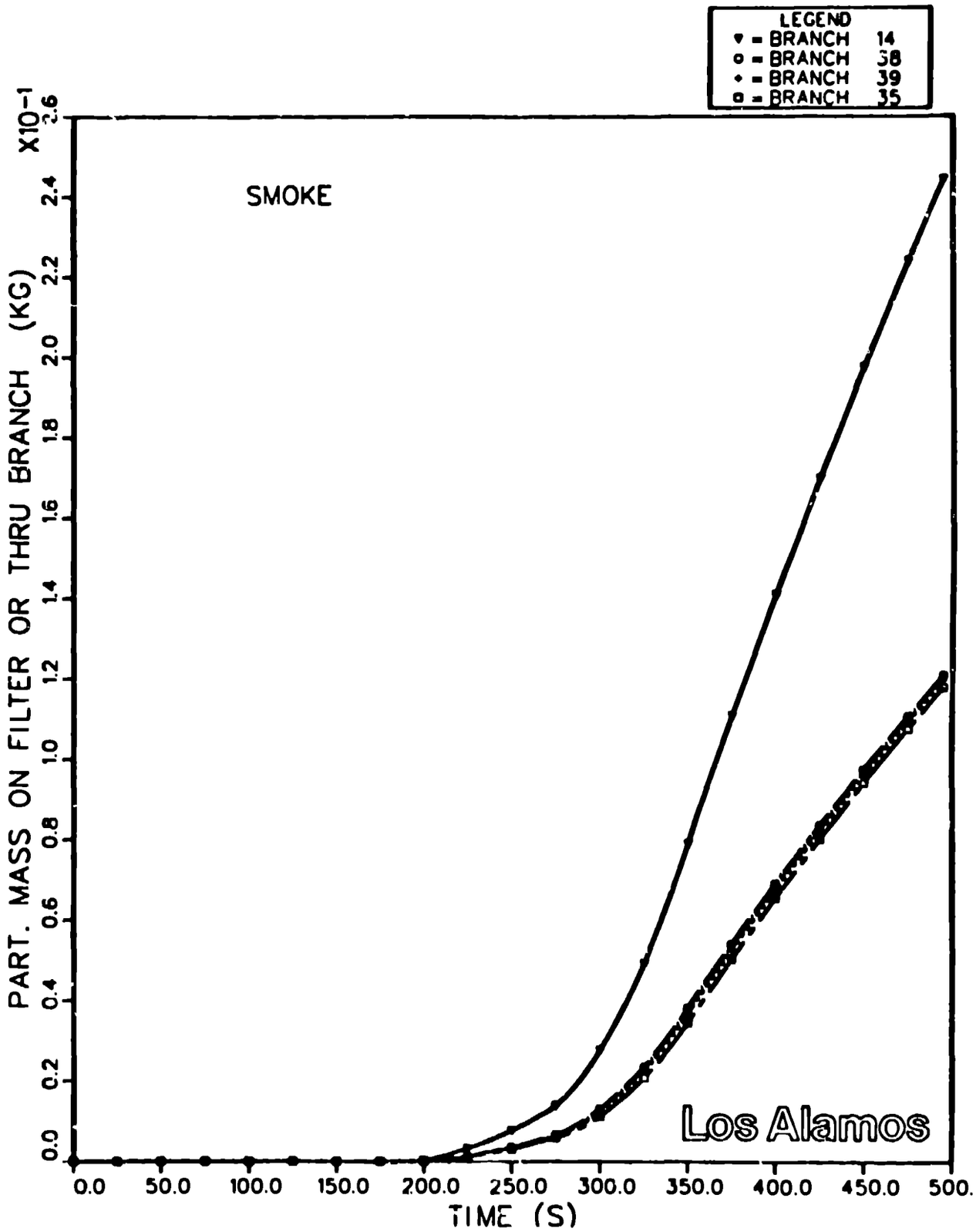

Figure 7. Accumulated smoke particulate mass for branches 14, 38, 39, and 35.

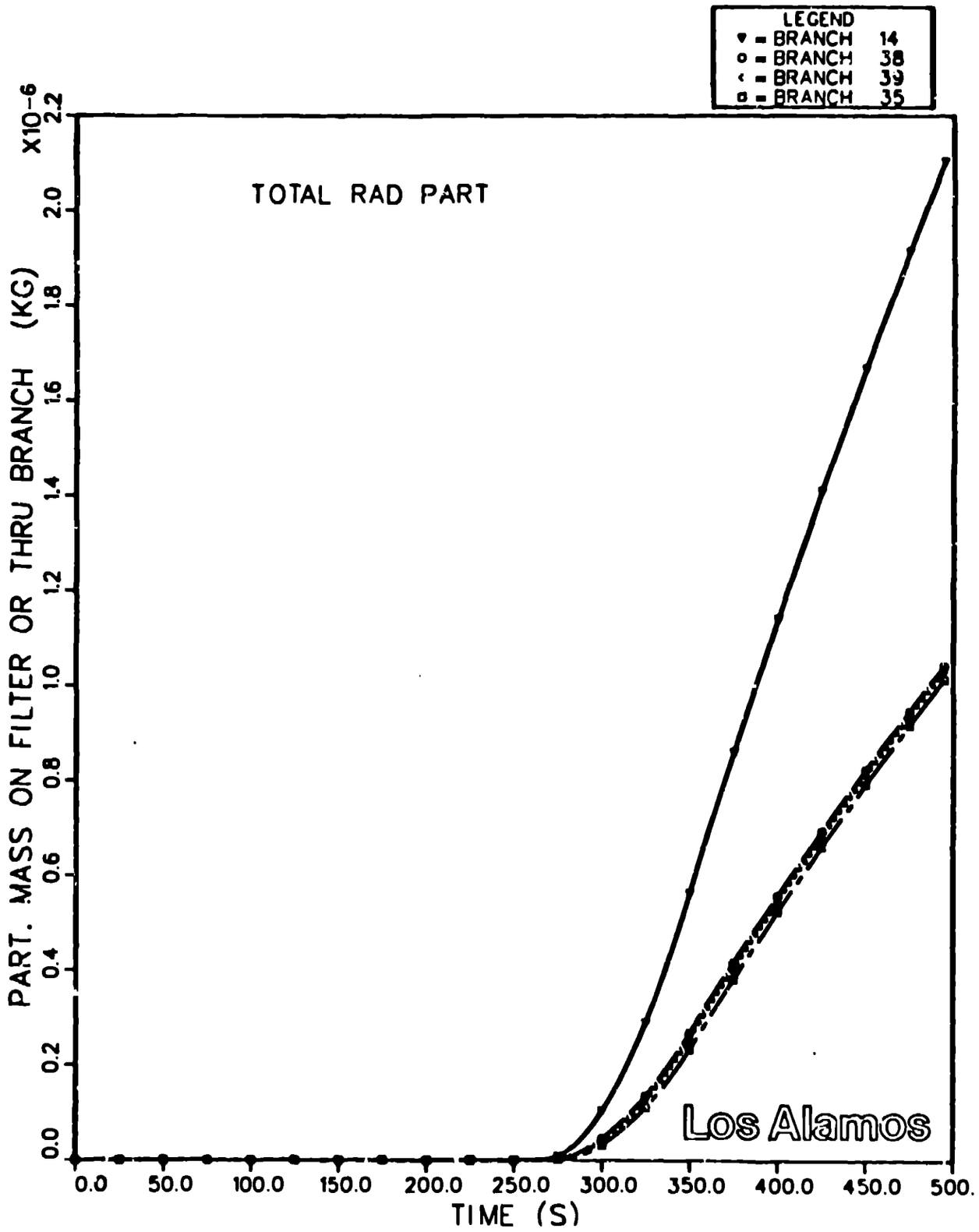

Figure 8. Accumulated radioactive particulate mass for branches 14, 38, 39, and 35.

Following the termination of the fire (350 s), the smoke and radioactive particulate flow rates begin to decrease as the particulate concentrations in the hot layer decrease and as the compartment exhaust flow rate decreases. The system gradually will reestablish the steady-state operating conditions.

An important result of any fire-induced transient is the calculated gas temperatures at various locations in the system. The temperature values are useful in assessing the damage to system components, especially HEPA filters. The temperature variation from the fire compartment to the facility exhaust is shown in Figure 9. As the warm gases are convected to the facility exhaust, convection and radiation heat losses occur in the duct components (branches 38 and 39). As a result of the heat losses, a decrease in gas temperature with increasing distance from the fire compartment is calculated.

Summary

The example calculation illustrated how the improved FIRAC code can be used to simulate a fire within a facility. Also, implementation of the FIRIN complex sequential burning option, the release of radioactive material by burning a contaminated combustible solid and the heating of a contaminated surface, the transport of smoke and radioactive particulates, and the internal boundary nodes representing the fire compartment were demonstrated. The example calculation also indicates how complicated the interpretation of the calculated results can become when several user options are enabled.

II. Full-scale Measurements of HEPA Filter Plugging and Particulate Deposition by Combustion Products

This section of the paper summarizes the results of experiments in two areas that were conducted by Los Alamos and New Mexico State University. The areas are (1) HEPA filter plugging by combustion aerosols[4] and (2) smoke transport and deposition in ventilation system ductwork.[5] In both cases, the work was part of Los Alamos' efforts to obtain experimental data to support FIRAC computer code development and verification.[1],[2],[6-8] A specialized facility was constructed to supply the needed experimental data.

Test Facility and Fuels

The test facility[9,10] was designed to supply experimental data for 0.61- by 0.61-m HEPA filters under conditions simulating those postulated as credible for fires in nuclear facilities. Industrial fires such as these are expected to differ from other kinds of fires in the types of materials involved and the ventilation conditions (availability of oxygen). A typical fuel mixture may be composed of the materials listed in Table 2.[7] These materials are likely to burn under both oxygen-rich and oxygen-starved conditions (over- and under-ventilated conditions) to produce particulate material, water vapor, and gaseous combustion products.

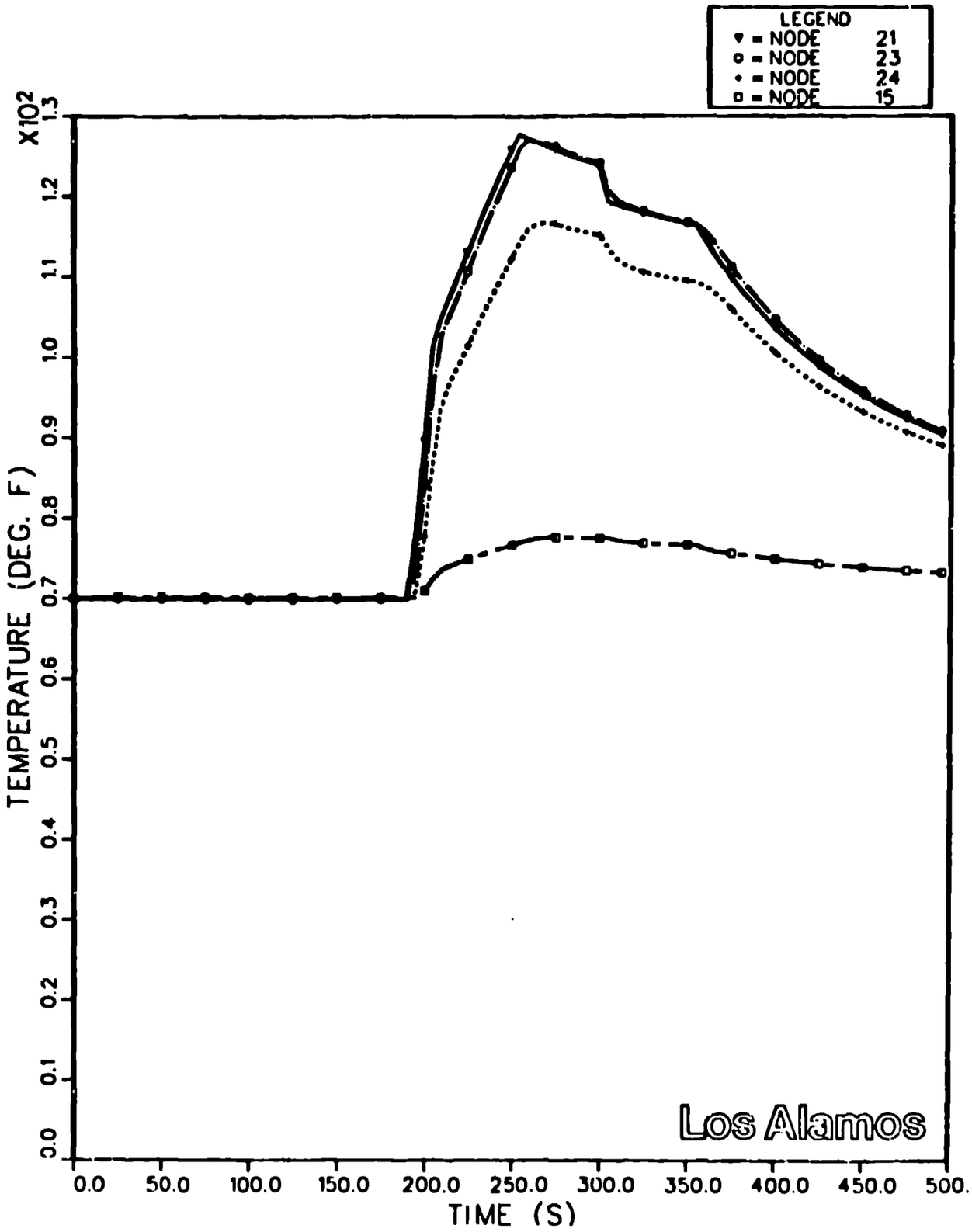

Figure 9. Calculated temperature history for nodes 21, 23, 24, and 15.

Table 2. Typical fuel mixture composition.

	Component	Composition (%)
1.	Polymethylmethacrylate	45
2.	Cellulosic	26
3.	Elastomer	18
4.	Polyvinyl Chloride	8
5.	Hydraulic Fluids	2
6.	Polystyrene	1

Some unique capabilities were required of the test facility. First, we needed the capability to burn fuels or mixtures of fuels listed in Table 2. Two pure materials were selected from Table 2, polystyrene (PS) and polymethylmethacrylate (PMMA). Although PS is not found in large proportions in nuclear fuel cycle facilities (PMMA is), it is the most severe smoke producer in Table 2. On the other hand, PMMA is known to produce relatively low quantities of smoke in comparison with the amount of mass burned. Hence, by selecting these two fuels we attempted to bracket the extremes of smoke generation--the mass fraction of solid or liquid fuel that converts to smoke--expected in plants. For liquid PS and PMMA burned at over-ventilated conditions, Tewarson[11] experimentally measured smoke mass fractions ($Y_s = m_s/m_b$) and got 0.33 and 0.021, respectively, where both the soot and low vapor pressure liquids are included in the aerosolized combustion products or "smoke." The quantities m_s and m_b are mass of smoke produced and mass of fuel burned, respectively.

To burn the fuels and control the burning efficiency, a special combustor was designed and manufactured for use in these studies by PNL.[12] The two mass burning rates were achieved by controlling the inlet air supply rate. Each burning rate was repeated two times. The repetitions were used to assess the reproducibility of the test results.

To obtain the filter plugging data,[4] we needed the capability to determine the accumulated mass gain of a clean 14-kg HEPA filter because of smoke and moisture clogging. Previous tests using polystryrene latex spheres led us to expect plugging (arbitrarily defined to be a 50% reduction in flow rate from the design value) to occur from an accumulation of under 500 g of dry solid material. We designed and constructed a special null-balance filter-weighing apparatus to resolve 2- to 3-g smoke accumulations out of 14 kg for a clean filter.

To obtain the deposition data,[5] the burn products had to be introduced into as long a duct as practical to enhance deposition and aerosol concentration changes for better resolution. We also needed to simulate rapid diffusion (mixing) of the smoke plume to make an upstream, centerline smoke concentration measurement. Finally, we needed special experimental apparatus suitable for making surface measurements of total aerosol mass deposition.

The facility described in References 9 and 10 was modified to facilitate the current experiments. The major modifications included

1. coupling to the combustion chamber,
2. the design and installation of a biplanar grid of round tubes to promote turbulent mixing,
3. the construction of a metal hot duct,
4. adding extra ductwork to bring the test section length for deposition up to about 45.6 ft (13.9 m), and
5. installation of specially designed nuclepore filter holders to collect deposition samples.

Instrumentation

Appropriate instrumentation was set up and calibrated to obtain measurements of the following.(4),(5)

1. Ambient pressure and temperature
2. Average or bulk volumetric airflow rate in the duct
3. Air temperature at four locations
4. Relative humidity
5. Fuel mass burning rate
6. Filter pressure drop
7. Filter incremental weight gain
8. Smoke mass concentration using two cascade impactors at two locations on the duct centerline [downstream of the mixing grid and 45.6 ft (13.9 m) further downstream]
9. Smoke size distribution using the same eight-stage cascade impactors to obtain the mass median aerodynamic diameter and geometric standard deviation (for a log-normally distributed aerosol)
10. Total mass deposition at one downstream location but on three surfaces (ceiling, one side wall, and floor) at the 45.6-ft (13.9-m) downstream mass concentration measurement location (See Item 6.)

Combustion Product Characterization

The characterization of the combustion products included only particulate constituents.(4),(5) The particulate combustion products were not monitored continuously, but rather intermittent samples were taken and analyzed.

Particulate mass concentrations (milligrams per cubic meter) were determined with Anderson Mark III stainless-steel in-stack inertial impactors incorporating straight nozzles. These impactors also measure aerodynamic particle diameter (based on unit density spheres) through seven stages of particle collection and a back-up filter. Pre-impactors for use in conjunction with the impactors were determined to be unnecessary for this application. Real-time particle sizing equipment also was used. The units used were a Royco Model 225 optical aerosol particle counter and a Thermal Systems Model 3030 electrical mobility analyzer. The real-time equipment was less suitable in this experiment because the particle size characteristics and mass concentration varied with the burn time.

Because about 1 min to 3 min of cycling time was required by each particle counter, respectively, the actual aerosol characteristics could not be resolved. In contrast, the inertial impactors were operated in such a manner (nozzle diameter and sampling time) to sample over the entire fuel burn. For this reason, the impactor size data are considered pertinent.

PS and PMMA combustion aerosol particulate size distributions were measured using the cascade impactors. The PS data are shown in Figure 10; this figure indicates that, for the high and low mass burning rates, the particle size distribution is nearly the same for particles less than 2.0μm. However, for particles greater than 2.0μm in diameter, there is a significantly greater relative number of particles at the higher burning rate compared with the lower burning rate. Also, the aerodynamic mean particle diameter varies from about 1.5 to 2.5 μm.

The change in particle size with transport along the 45.6-ft (13.9-m) length can be observed in Figure 10. With the exception of the larger (greater than 2.0μm) particles, no clear shift in size distribution occurs. However, with these PS particles, the upstream size distribution by aerodynamic diameter relative to the corresponding downstream data of the same test suggests an average particle size reduction of about 1 μm.

The volumes of soot particles generated by the burner for the two fuels were measured using the Royco counter. The main features observed were large variations of soot particle output rates and variations from burn to burn under the same conditions. Peak volumetric output rates for the PS and PMMA fuels varied by more than an order of magnitude. Similar particle size data for PMMA are presented in Reference 5. These data show that the mass median aerodynamic diameter of PMMA was significantly smaller than that of PS--about 0.7 to 1.0 μm.

HEPA Filter Plugging by Combustion Aerosols

The experimental results reported here represent a continuation of work reported at the 17th DOE Nuclear Air Cleaning Conference.(1),(8)

Exposing a HEPA filter to heat and smoke significantly alters its operating characteristics.(2),(6),(8),(13),(14) This investigation focused on the characteristics that relate to filter plugging or to the increase in pressure drop across a filter as a result of the collection of particulate material on the filtration media. Such information is required to better understand how filters are plugged with combustion-generated aerosols, and it will improve our FIRAC-based estimates of ventilation system response to compartment fires.

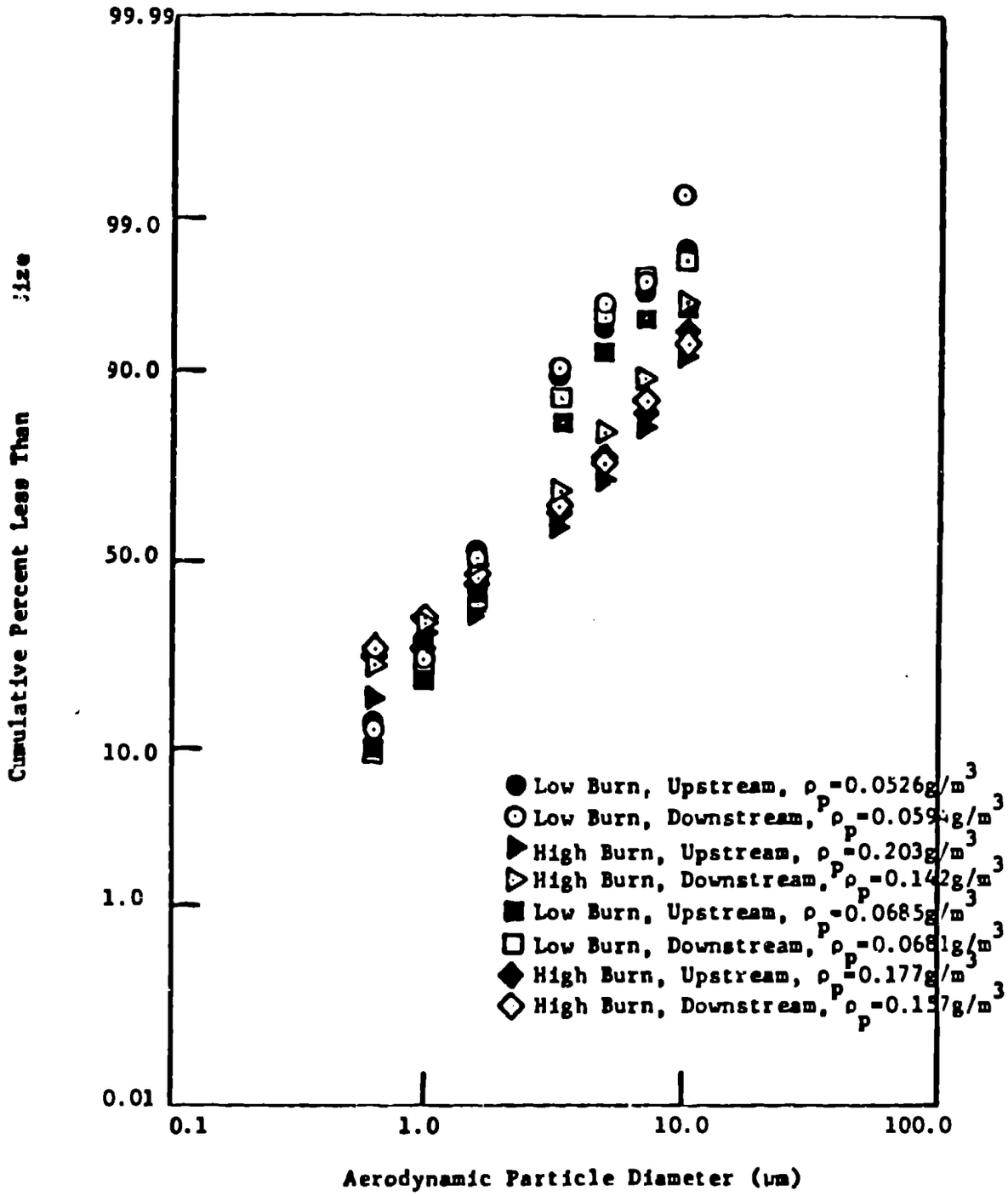

Figure 10. Polystryene combustion smoke particle size distribution.

Specific questions about the problem we investigated included the following.

1. What is the correlation between accumulated combustion particulate mass on the HEPA filter and flow resistance across the filter?
2. What is the effect of the soot fraction (as manifested by fuel type) on HEPA filter plugging?
3. What is the effect of fuel mass burning rate on HEPA filter plugging?
4. What is the penetration of the aerosols within the filtration medium?
5. Does the HEPA filter upstream faceguard influence HEPA filter plugging?
6. Does the mechanism causing plugging vary from fuel to fuel?

Table 3 summarizes conditions associated with combustion of the filter plugging test fuels. Results for both fuels are given in Table 4. These data are the result of burning many cups of fuel in each case, and thus the mass burning rates are average values. The HEPA filters tested with PS had protective metal face screens (1-cm by 1-cm mesh size) with the exception of filters numbered 6 and 7. The HEPA filters tested with PMMA all had the metal screens removed.

The details of the plugging process for each filter are shown in Figure 11. The actual resistance, R or W, is normalized by the initial clean filter resistance. The data shown the influence of the PS mass burning rate on the quantity of the particulate material collected that is necessary for plugging. From Figure 11, the importance of the protective screen on HEPA filter plugging can be seen to be negligible. Similar data for PMMA are presented in Reference 4.

Rather than trying to construct any realistic physical mechanism for the cause of plugging, we propose a phenomenological approach as follows.[2],[4],[6]

$$\frac{W}{W_o} = F(M_p) \quad ,$$

where $W = \Delta p/Q$ is the resistance coefficient. W_o is the value of W for a clean filter, Δp is pressure differential, and Q is volumetric flow rate. F is a monotonically increasing functon of M_p, which is the total mass of particulate accumulated on the filter and is the relative resistance. To satisfy the clean filter requirement, we must have

$$F(M_p = 0) = 1.$$

Table 3. Test fuel combustion conditions.

Fuel	Chemical Formula	Combustion Efficiency	Stoichiometric Airflow Rate (m^3/h)	Ratio of Actual to Stoichiometric Airflow Rates	Comments
PS (granular)	CH	0.6	7.4	0.23	Low Burn Rate, Underventilated
				0.93	High Burn Rate, Underventilated
PMMA	$CH_{1.6}O_{0.4}$	0.9	4.0	0.85	Low Burn Rate, Underventilated
				2.1	High Burn Rate, Overventilated

Table 4. Summary of combustion products plugging of HEPA filters.

Fuel	Test No.	Clean Static Pressure Drop (cm w.g.)	Apparent Mass Burning Rate (g/min)	Total Particulate Mass Collected at Plugging* (g)
PS	1	2.1	19.4 (high)	527
PS	2	2.1	21.3 (high)	432
PS	3	2.1	15.4 (low)	1256
PS	4	2.0	21.7 (high)	405
PS	5	2.1	17.5 (low)	1207
PS	6	2.1	22.9 (high)	432
PS	7	2.1	21.3 (high)	391
PMMA	8	2.2	11.6 (high)	233
PMMA	9	2.2	12.4 (low)	257
PMMA	10	2.2	15.6 (high)	186
PMMA	11	2.2	13.4 (low)	309

*The HEPA filter resistance ratio has a value of 12.0 for each filter.

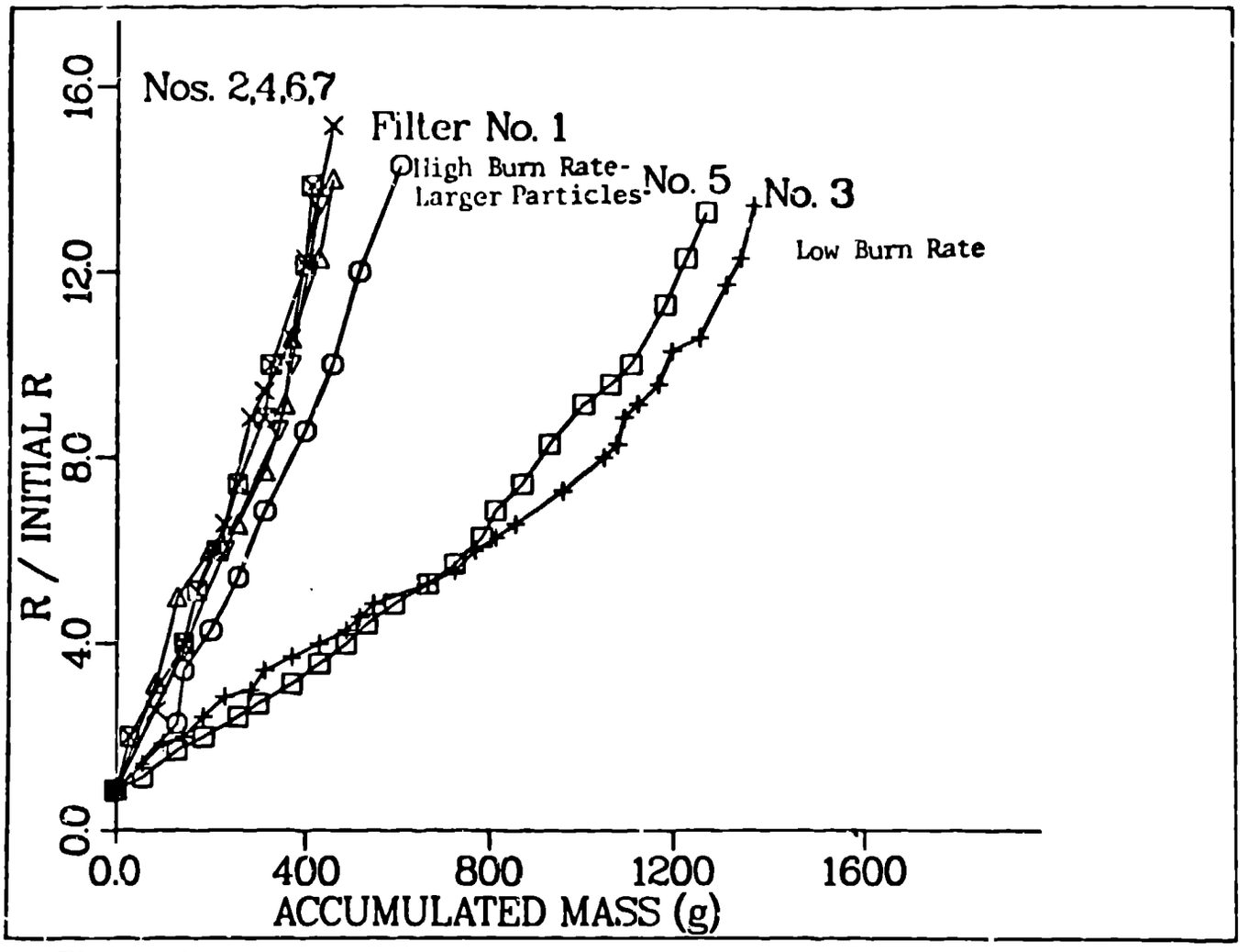

Figure 11. Variation of resistance ratio with accumulated mass for polystyrene combustion.

We believe the following expression should be adequate for all practical purposes.

$$F = 1 + \alpha M_p + \beta M_p^2 \quad ,$$

where α and β are two coefficients determined by experimentation. Their evaluation from data such as that shown in Figure 11 forms the basis of the filter plugging test program.

Table 5 shows the values for α and β obtained by curve-fitting techniques for the combustion conditions tested. The resistance ratio is observed to be a strong function of the linear term in M_p -- the β values are relatively small. The filter plugging coefficients given in Table 5 can be used in the input data deck of the Los Alamos fire accident analysis computer code FIRAC. An equation for F(Mp) in the code allows the user to simulate an infinite range of plugging conditions depending on the values of α and β input.

Table 5. Compilation of HEPA filter resistance ratio.
FUNCTION* COEFFICIENTS

Fuel	Combustion Condition	α	β
PS	High O_2 (Underventilated)	0.022248	0.64249×10^{-6}
PS	Low O_2 (Underventilated)	0.0057105	0.17108×10^{-5}
PMMA	Underventilated	0.0476796	-0.30826×10^{-4}
PMMA	Overventilated	0.0641064	-0.57276×10^{-4}

*The HEPA filter resistance ratio has a value of 12.0 for each filter.

Particle size data were used in Reference 4 to explain the variation in PS combustion particulate mass necessary to plug the HEPA filters. In Reference 4, we showed that the particles greater than 2.0 μm in diameter dominate the plugging of the filter. Particles less than 2.0 μm apparently penetrate the filter medium and contribute to the mass of collected particulate material but contribute little to increase the static pressure drop across the filter. Removal of the HEPA filters from the test apparatus supports this speculation because the upstream face had a thick "mat" of fragile particulate material that tended to fall off the filter even when disturbed by the most careful handling.

Tentative qualitative conclusions can be made regarding the plugging characteristics involving particulate mass concentration and accumulated particulate mass on the filter.

- Normalized HEPA filter flow resistance can be correlated with the accumulated mass gain on the filter for a given combustion aerosol (PS and PMMA). When the combustion conditions change (fuel and/or oxygen availability), the HEPA filter plugging characteristics change and are explained with the particulate mass concentration for particles greater than 2.0 μm.
- For these PS and PMMA tests, the lower the fuel soot fraction, the smaller the accumulated mass gain on the HEPA filter required for plugging. This results from the physical characteristics of the particulate material--mass concentration and particle size. Evidently, for PS and PMMA, a different physical mechanism was responsible for the plugging.

Smoke Transport and Deposition in Ventilation System Ductwork

Although intuition might suggest that aerosol losses because of deposition are insignificant, a previous study has indicated that such losses can be appreciable in mass percentage. Qualitative cascade impactor measurements in the duct downstream of the full-sized compartment fire test facility at Lawrence Livermore National Laboratory (LLNL) have indicated that as much as 60% of combustion product aerosol mass can be removed by deposition in a relatively short (about 32-ft-long) duct.[13] In case of a fire in a nuclear facility, the presence of combustion products poses a threat to the

HEPA filters.(1),(2),(6),(7),(8),(13),(14) A reduction in smoke concentration because of deposition can delay filter plugging. Because deposition is size dependent,[6] it also can modify the size distribution function of the smoke challenging the filters.

Further, for fuel cycle facilities under fire accident conditions, the smoke (solid and liquid aerosol) could be contaminated with radioactive material. In this case it becomes important to know where hazardous material is deposited within the plant ventilation system. A reduction in airborne material concentrations will reduce the quantity of radioactive material accumulating on the HEPA filters and passing through them. We are particularly interestesd in the location and concentration of radioactive material in the respirable size range, namely, about 0 to 15 μm. This time- and location-dependent concentration will be continually changing because of deposition and material interaction (coagulation).

For these reasons there is a need to check (under realistic conditions) the accuracy of deposition equations available in the literature. Some of these idealized deposition equations currently are being used to compute unsteady material depletion in FIRAC and other Los Alamos accident analysis computer codes.[2,6] However, at this stage of computer code development, we have relatively little confidence in the predictions of deposition losses for combustion aerosols.

In this study we performed smoke transport and deposition tests under realistic conditions using real combustion products (particulate and gaseous, including water vapor) in full-sized ducts at typical airflow rates. We are unaware of adequate data of this kind in the available literature.[5] With such depletion/modification data we can help answer three questions for realistic fire conditions.

1. How important is deposition; that is, how much material accumulates on the walls?
2. How much change in smoke characteristics (concentration and size distribution) can occur over reasonable duct lengths?
3. Are our idealized equations from the literature giving us reasonable, and preferably conservative, quantitative estimates of deposition?

Table 6 summarizes the numerical data obtained during the duct wall deposition tests. In these tests, the accumulated particulate mass on the HEPA filters and actual particulate mass deposits at the duct wall were measured in addition to the physical characteristics of the airborne particles as already described. The values reported for the duct volumetric flow rate are arithmetic averages of the flow at the initiation and conclusion of each test.

The particulate mass concentration data, in conjunction with the mass burning rate given in Table 6, imply an important feature associated with PS combustion. This feature is that the total particulate mass concentration measured near the HEPA filter is proportional

to the mass burning rate. This is established by ratioing the average high burning rate to the average low burning rate and obtaining the value of 2.0. Calculating the corresponding ratio for average total particulate mass concentrations gives 2.3. The correspondence (deviation from mean less than 7%) implies a constant soot fraction for underventilated conditions.

The effect of the 45.6-ft (13.9-m) transport length on duct centerline particulate mass concentration is summarized in Table 7. The

Table 6. Duct wall deposition experimental data.

Fuel Type	Burn Condition	Fuel Mass Burned (g)	Total Time Time (min)	Fuel Mass Burn Rate, $\dot{m}_b$ (g/min)	Volumetric Duct Air Flow Rate, Q(m^3/h)
PS	1.7 m^3/hr Combustion Air Low Burn Rate, Underventilated	200.7	21.9	9.16	1642
PS	1.7 m^3/hr Combustion Air Low Burn Rate, Underventilated	250.0	29.7	8.96	1470
PS	6.8 m^3/hr Combustion Air High Burn Rate, Underventilated	250.0	14.35	17.42	1589
PS	6.8 m^3/hr Combustion Air High Burn Rate, Underventilated	250.3	13.60	18.40	1439
PMMA	3.4 m^3/hr Combustion Air Low Burn Rate, Underventilated	600.5	50.1	12.0	1607
PMMA	3.4 m^3/hr Combustion Air Low Burn Rate, Underventilated	600.0	52.4	11.48	1448
PMMA	8.5 m^3/hr Combustion Air High Burn Rate, Overventilated	1000.3	81.9	12.26	1700
PMMA	8.5 m^3/hr Combustion Air High Burn Rate, Overventilated	1000.0	85.6	11.70	1530

Table 6. (Cont.)

Fuel Type	Burn Condition	Upstream Impactor Conc. (g/m^3)	Downstream Impactor Conc. (g/m^3)	Accumulated HEPA Mass Gain (g)	Wall Nuclepore Filter Mass Deposit (mg) Top	Side	Bottom
PS	1.7 m^3/h Combustion Air Low Burn Rate, Underventilated	0.0526	0.0594	14.76	0.2	0.2	1.1
PS	1.7 m^3/h Combustion Air Low Burn Rate, Underventilated	0.0685	0.0681	32.3	0.1	0.1	0.8
PS	6.8 m^3/h Combustion Air High Burn Rate, Underventilated	0.2027	0 1415	71.02	0.02	0.3	1.5
PS	6.8 m^3/h Combustion Air High Burn Rate, Underventilated	0.1765	0.1566	65.0	0.2	0.4	1.4
PMMA	3.4 m^3/h Combustion Air Low Burn Rate, Underventilated	0.0154	0.0150	22.9	0.1	0.1	0.4
PMMA	3.4 m^3/h Combustion Air Low Burn Rate, Underventilated	0.0202	0.0157	13.0	0.0	0.1	0.4
PMMA	8.5 m^3//h Combustion Air High Burn Rate, Overventilated	0.0045	0.0038	5.43	0.1	0.1	0.4
PMMA	8.5 m^3/h Combustion Air High Burn Rate, Overventilated	0.0051	0.0048	5.64	0.0	0.1	0.3

Table 7. Variation of particulate mass concentration by transport*.

Fuel	Combustion Condition	$\left(\frac{\rho_p}{\rho_{po}}\right)_{exp.}$	$\left(\frac{\rho_p}{\rho_{po}}\right)_{theo.}$
PS	high	0.70	0.81
PS	high	0.89	0.89
PS	low	1.13	0.83
PS	low	0.99	0.84
PMMA	overventilated	0.84	0.89
PMMA	overventilated	0.94	0.75
PMMA	underventilated	0.97	0.75
PMMA	underventilated	0.78	0.86

* Duct length (from impactor to impactor) was 13.9 m.

last two columns give calculations of ρ_p/ρ_{po}, the particulate mass concentration ratio at the two impactors, for the experiments and the theory based only on gravitational settling. Note that the averages of each of the four conditions are predicted by the theory with an error of less than 10% (based on averages) with the exception of the PS low burning rate condition where the experimental result should be rejected.

Experimental deposition results have been compared with predictions with gravitational settling theory (currently being used in FIRAC) in Table 8. The important operational conditions are given to identify each test. Under the columns labeled "Experimental Data," the experimental results alone are presented where the final result is a particulate mass ratio, m_d/m_b. This ratio is the mass deposited on duct walls divided by the initial mass of unburned fuel. The mass deposited on the walls, m_d, is given by

$$m_d = Y_s m_b - m_f,$$

where m_f is the accumulated particulate mass on the HEPA filter for the fuel burned. The ratio m_d/m_b identifies that portion of the fuel mass that was deposited on the walls. The m_d calculations assume a constant value for Y_s (0.33 for PS and 0.021 for PMMA) regardless of the burning condition. This mass-balance calculation for m_d using data from Reference 11 for Y_s did not resolve wall mass deposition for the underventilated PMMA burn rate.

Table 8. Experimental deposition results compared to gravitational settling theory predictions.

Fuel Type	Burn Condition	Fuel Mass Burned, m_b(g)	$m_p J_p$ $\left(\frac{g\,m}{m^2\,h}\right)$	U_{pe} $\left(\frac{m}{h}\right)$	ρ_{pce} $\left(\frac{g}{m^3}\right)$	Accumulated HEPA Mass Gain, m_f(g)
PS	Low	200.7	2.66	44.8	1.10×10^{-1}	14.8
PS	Low	250.0	1.43	21.0	1.21×10^{-1}	32.3
PS	High	250.0	5.53	39.1	2.17×10^{-1}	71.0
PS	High	250.3	5.44	34.7	2.53×10^{-1}	65.0
PMMA	Low	600.5	0.422	28.1	9.42×10^{-3}	22.9
PMMA	Low	600.0	0.808	51.5	9.96×10^{-3}	13.0
PMMA	High	1000.3	0.258	67.9	9.06×10^{-3}	5.43
PMMA	High	1000.0	0.185	38.5	9.66×10^{-3}	5.66

Table 8. (Cont).

		Gravitational Settling Theory				Experimental Data		
Fuel Type	Burn Condition	m_{dg}	$\frac{m_{dg}}{m_b}$	Total Mass Accounted (g)	Apparent Soot Fraction Y_{sa}	$m_b Y_s$	$m_d \cdot Y_s m_b - m_f$	$\frac{m_d}{m_b}$
PS	Low	17.8	0.0887	32.6	0.16	66.2	51.4	0.256
PS	Low	13.4	0.0536	45.7	0.18	82.5	50.2	0.201
PS	High	20.4	0.0816	91.4	0.27	82.5	11.5	0.046
PS	High	20.0	0.0799	85.0	0.34	82.6	17.6	0.070
PMMA	Low	2.31	0.0385	25.2	0.042	12.6	-10.3	----
PMMA	Low	4.24	0.0707	17.2	0.029	12.6	-0.4	----
PMMA	High	7.76	0.0776	13.2	0.013	21.0	15.6	0.0156
PMMA	High	5.31	0.00531	11.0	0.011	21.0	15.4	0.0154

Comparing the predicted and experimental PS combustion aerosol deposition quantities in Table 7 suggests that, within a factor of 2 or 3, the values of m_{dg}/m_b agree. This level of agreement weakly supports the gravitational settling theory. In addition, the calculated or apparent PS soot fraction, Y_{sa}, is within 12% of the 0.33 value at the high burn rate. This confirms Y_s for the PS fuel at these conditions. For the low burn rate conditions, the Y_{sa} values are significantly lower than the assumed Y_s value of 0.33. With the PMMA tests, comparisons can be made only for the overventilated combustion condition (m_d is negative for the underventilated condition). Again, the mass ratios and soot fractions agree to a factor of 3 or less. However, the consistency of Y_{sa} data suggests that Y_s is indeed different for the two conditions--by a factor of at least 2 for these experiments.

Gravitational settling is accompanied by other deposition mechanisms in a horizontal duct and includes turbulent and Brownian diffusion, inertial impaction, and electrostatic effects. For the horizontal straight duct used in these experiments, inertial and electrostatic effects were not significant. Considerations of other deposition mechanisms, including calculations and comparisons with the data obtained in the current study, have been made elsewhere.[4,5-7]

The deposition rates predicted by theory are not fully supported by the experimental data. Two reasons for this are the preliminary, and thus relatively crude, nature of the particle deposition experiments and the simplistic theoretical model used in FIRAC at present. Further, because the mean particle diameters determined by the impactors are much too small, the gravitational settling theory currently used by FIRAC is not conservative, but rather significantly underpredicts the actual particulate mass deposition rates of the combustion aerosols tested. Successful particle deposition studies where theory and experimental results are mutually supportive will require improved theoretical developments incorporating additional deposition mechanisms and improved experimental techniques and procedures.

The conclusions developed from this experimental work involving deposition of combustion products of PS and PMMA fuel are as follows.

1. Particulate mass deposition is an important feature associated with the flow of combustion products and, even for short duct lengths (31 hydraulic diameters), may reach 25% of the unburned fuel as with PS.

2. Physical changes associated with the transport of the particulate combustion products include a 10 to 30% reduction in mass concentration and a small (~1 μm) reduction in particle size only observable for the PS combustion particles with an aerodynamic diameter greater than 2.0 μm.

3. Comparisons of the experimental results with the theory incorporating gravitational settling provide some preliminary checks.

4. The experimental techniques used in this effort are not sufficiently sensitive to verify the deposition models described.

Because HEPA filter plugging rates and efficiencies are dependent on the airborne particulate mass and size distributions arriving at the filter, deposition is an important consideration. The experimental work performed here establishes some support for the theory developed and used by FIRAC. However, improved experiments directed at the deposition problem alone are required to establish the important deposition mechanisms that should be included in the FIRAC code.

REFERENCES

1. R. W. Andrae, J. W. Bolstad, W. S. Gregory, F. R. Krause, R. A. Martin, P. K. Tang, M. Y. Ballinger, M. K. W. Chang, J. A. Glissmeyer, P. C. Owczarski, J. Mishima, S. L. Sutter, E. L. Compere, H. W. Godbee, and S. Bernstein, "Methods for Nuclear Air Cleaning System Accident Consequence Assessment," Proc. 17th DOE, Nuclear Air Cleaning Conference, Denver, Colorado, August 2--5, 1982.

2. R. W. Andrae, J. W. Bolstad, M. Burkett, W. S. Gregory, R. A. Martin, and P. K. Tang, "FIRAC Users Manual - A Computer Code for Analysis of Fire-induced Flow and Material Transport in Nuclear Facilities," Los Alamos National Laboratory report in preparation.

3. M. K.Chan, M. Y. Ballinger, P. C. Owczarski, and S. L. Sutter, "User's Manual for FIRIN1: A Computer Code to Characterize Accidental Fire and Radioactive Source Terms in Nuclear Fuel Cycle Facilities," Battelle Pacific Northwest Laboratory report PNL-4532 NUREG/CR-3037, (December 1982).

4. D. L. Fenton, M. V. Gunaji, W. S. Gregory, and R. A. Martin, "Investigation of High-efficiency Particulate Air Filter Plugging by Combustion Aerosols," Los Alamos National Laboratory report in preparation.

5. R. A. Martin and D. L. Fenton, "Full-scale Measurements of Smoke Transport and Deposition in Ventilation System Ductwork," Los Alamos National Laboratory report in preparation.

6. R. A. Martin, P. K. Tang, A. P. Harper, J. D. Novat, and W. S. Gregory, "Material Transport Analysis for Accident-induced Flow in Nuclear Facilities," Los Alamos National Laboratory report LA-9913-MS, NUREG/CR-3527 (October 1983).

7. "Fuel Cycle Facility Accident Analysis Handbook," Los Alamos National Laboratory report LA-9180M, NUREG/CR-2508, PNL-4149 in preparation.

8. W. S. Gregory, R. A. Martin, P. R. Smith, and D. L. Fenton, "Response of HEPA Filters to Simulated Accident Conditions," Proc. of the 17th DOE Nuclear Air Cleaning Conference, Denver, Colorado, August 2--5, 1982.

9. D. L. Fenton, J. J. Dallman, P. R. Smith, R. A. Martin, and W. S. Gregory, "The Los Alamos National Laboratory/New Mexico State University Filter Plugging Test Facility--Description and Preliminary Test Results," Los Alamos National Laboratory report LA-9929-MS, NUREG/CR-3242 (October 1983).

10. . J. Dallman, "HEPA Filter Loading by Simulated Combustion Products," Masters Thesis submitted to Mechanical Engineering Department, New Mexcio State University (Las Cruces, New Mexico, 1982).

11. A. Tewarson, "Physico-Chemical and Combustion Pyrolysis Properties of Polymeric Materials," Factory Mutual Research Corp. Technical Report FMRC J. I. OEON6.RC ·C80-T-79 (November 1980).

12. M. K. W. Chan, "Testing and Calibration Results of the Filex Smoke Generators," Pacific Northwest Laboratory draft report (March 30, 1982).

13. N. Alvares, D. Beason, W. Bergman, J. Creighton, H. Ford, and A. Lipska, "Fire Protection Countermeasures for Containment Ventilation," Lawrence Livermore National Laboratory progress report UCID-18781 (September 1980).

14. W. Bergman, H. Hebard, R. Taylor, and B. Lum, "Electrostatic Filters Generated by Electric Fields," Lawrence Livermore National Laboratory paper UCRL-81926 (July 1979), submitted to Second World Filtration Congress (London, September 18--20, 1979).